Supporting Information

Palacios-Prado et al. 10.1073/pnas.1004552107

SI Text

Cells and Culture Conditions. Experiments with homotypic junctions were performed on HeLa cells (ATCC CCL2) transfected with wild-type connexin45 (Cx45), its fusion form with green fluorescent protein tagged to the C terminus (Cx45-EGFP), or connexin43 (Cx43)-EGFP. Experiments with heterotypic junctions were performed on cocultures of HeLa cells expressing wild-type Cx45 or Cx43-EGFP. Cells were grown in Dulbecco's modified Eagle medium supplemented with 10% FCS. The cells were passaged weekly by 1:10 dilution and maintained in a 95% O_2–5% CO_2 moist atmosphere at 37 °C. All media and culture reagents (GIBCO-BRL) were obtained from Life Technologies. The transfection procedure has been described previously (1).

Electrophysiological and Fluorescence Measurements. For simultaneous electrophysiological and fluorescence recording, cells grown on glass coverslips were transferred to an experimental chamber with constant flow-through perfusion mounted on the stage of an Olympus IX70 inverted microscope (Olympus America) equipped with a Hamamatsu cooled digital camera and UltraView fluorescence imaging system (Perkin-Elmer Life Sciences). Appropriate excitation and emission filters (Chroma Technology) were used to image EGFP and 2,7-bis(2-carboxyethyl)-5(6)-carboxyfluorescein (BCECF). Junctional conductance, g_j, was measured in selected cell pairs by dual whole-cell patch clamp. Each cell of a pair was voltage clamped independently with a separate patch clamp amplifier EPC8 (HEKA Elektronik). Voltages and currents were digitized using a MIO-163 A/D converter (National Instruments) and acquired and analyzed using custom-made software (2). The voltage in cell 1 (ΔV_1) was stepped while the voltage in cell 2 was kept constant, and junctional current (I_j) was measured as the negative of the change in current in cell 2, $I_j = -\Delta I_2$. Junctional conductance (g_j) was given as $-I_j/\Delta V_1$. To reduce effects of series resistance on measurements of g_j (3), we selected cell pairs exhibiting small junctional plaques (JP) (< 4 μm in diameter) and used patch pipettes with resistances below 5 MΩ. Typically, cell pairs without JPs showed no electrical coupling. Experiments were performed at room temperature in modified Krebs-Ringer (MKR) solution, composition (in mM): NaCl, 140; KCl, 4; $CaCl_2$, 2; $MgCl_2$, 1; glucose, 5; pyruvate, 2; Hepes, 5 (pH 7.4). Patch pipettes were filled with saline containing (in mM): KCl, 130; sodium aspartate, 10; $MgCl_2$, 1; $CaCl_2$, 0.2; EGTA, 2; Hepes, 5 (pH = 7.2). Ammonium chloride (NH_4Cl) or CO_2 was used to increase or reduce the intracellular pH (pH_i).

Fluorescence Imaging Studies. Fluorescence signals were acquired using UltraVIEW software for image acquisition and analysis (Perkin-Elmer Life Sciences). For pH_i measurement, cells were loaded introducing the unesterified form of BCECF (8 μM) into the cells through patch pipettes in whole-cell voltage clamp mode. Dye was excited alternately with low-intensity 436-nm and 500-nm light for 0.5 s every 15 s (to minimize photobleaching), and the emitted light was filtered at 540 nm. The emitted light from 500-nm excitation is pH sensitive, whereas that from 436-nm excitation is much less pH sensitive, so that the ratio of emitted light at the two excitation wavelengths is a function of pH_i. All experiments were performed at room temperature. We found no difference in fluorescence intensity over time when images were acquired once every 20 s or every 5 s, indicating that dye bleaching was minimal. In our studies we typically observed less than ~5% decay of emitted light intensity over 1 h of measurement. In addition, during whole-cell recording conditions, unbleached BCECF molecules can diffuse from the pipette into the cell, perhaps accounting for the low level of bleaching. Moreover, it is well established that ratiometric measurements are relatively insensitive to bleaching effects.

Statistical Analysis. The analysis was performed using SigmaPlot software, and averaged data are reported as the means ± SEM.

1. Kreuzberg MM, et al. (2005) Functional properties of mouse connexin30.2 expressed in the conduction system of the heart. *Circ Res* 96:1169–1177.
2. Trexler EB, Bukauskas FF, Bennett MVL, Bargiello TA, Verselis VK (1999) Rapid and direct effects of pH on connexins revealed by the connexin46 hemichannel preparation. *J Gen Physiol* 113:721–742.
3. Wilders R, Jongsma HJ (1992) Limitations of the dual voltage clamp method in assaying conductance and kinetics of gap junction channels. *Biophys J* 63:942–953.

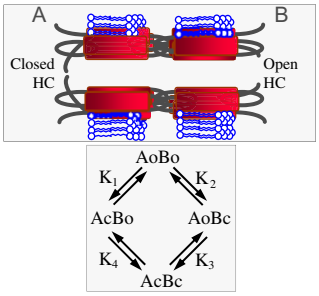

Fig. S1. Schematics of the GJ channel containing A and B hemichannels, each with its own fast gate at the cytoplasmic end of the channel. At the bottom is shown the scheme of transitions in the four-state model. AoBo: both gates are open; AcBo: gate A is closed, and gate B is open; AoBc: gate A is open, and gate B is closed; and AcBc: both gates are closed. Transitions between adjacent states are described by equilibrium constants, $K_i = e^{Ai*(\Pi*Vj,H-Vo,H,i)}$ (i = 1–4), where A_i is the voltage sensitivity coefficient, $V_{j,H}$ is the voltage across hemichannel, $V_{o,H,i}$ is the voltage at which occupation of the two states is equal, and Π is a gating polarity. The two gates are in series and operate in a contingent manner in which voltage across one gate depends on the state of series gate. The state of each gate (open/residual) was determined stochastically by the fraction of transjunctional voltage (V_j) that falls across each hemichannel. The model allows for the input of unitary conductances of open and residual states, which rectifies $\gamma = \gamma_o \cdot e^{VjH/R}$, where γ_o is conductance at $V_{jH} = 0$, and R is a rectification coefficient. The simulation typically requires ~10 s to calculate g_j–V_j plots for a junction containing 1,000 channels. (This figure was modified from figure 5 in ref. 1).

1. Paulauskas N, Pranevicius M, Pranevicius H, Bukauskas FF (2009) A stochastic four-state model of contingent gating of gap junction channels containing two "fast" gates sensitive to transjunctional voltage. *Biophys J* 96:3936–3948.

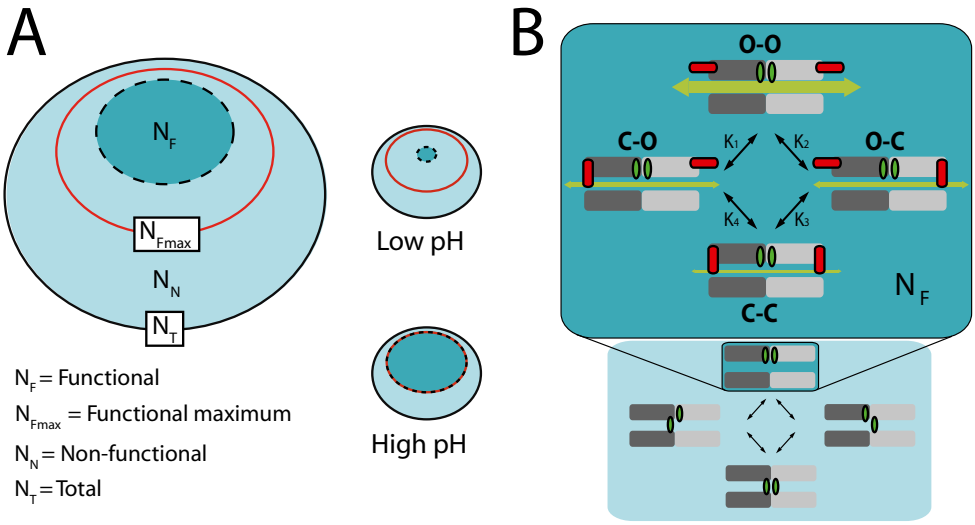

Fig. S2. (*A*) Venn diagram in which the total number (N_T) of gap junction (GJ) channels is composed of the maximum number of functional channels (N_{Fmax}) and nonfunctional (N_N) channels. Functional channels (N_F) operate in response to V_j and their number changes depending on pH_i. N_N channels are permanently closed. N_{Fmax} was estimated from the maximum N_F measured at intracellular pH (pH_i) > 8. at $V_j = 0$. Small Venn diagrams illustrate changes of N_F depending on pH_i. (*B*) Schematic of N_F GJ channels with slow (green) and fast (red) gates in open or closed states for the right (light gray) and left (dark gray) hemichannels of the GJ channel. In N_F channels both slow gates are open, and the fast gates may be open or closed. N_F channels can dwell in four different states [open-open (O-O), both aHCs open; open-closed (O-C) and closed-open (C-O), one aHC open and one closed; and closed-closed (C-C), both aHCs closed] depending on the state of the fast gates, resulting in three possible conductances: γ_o for O-O, residual conductance (γ_{res}) for O-C and C-O, and γ_{res2} (for C-C). K_i (i = 1–4) are equilibrium constants of transitions between adjacent states. If one of the slow gates is closed, then the channel is fully closed. At alkaline pH_i all N_F channels are open, and $N_F = N_{Fmax}$.

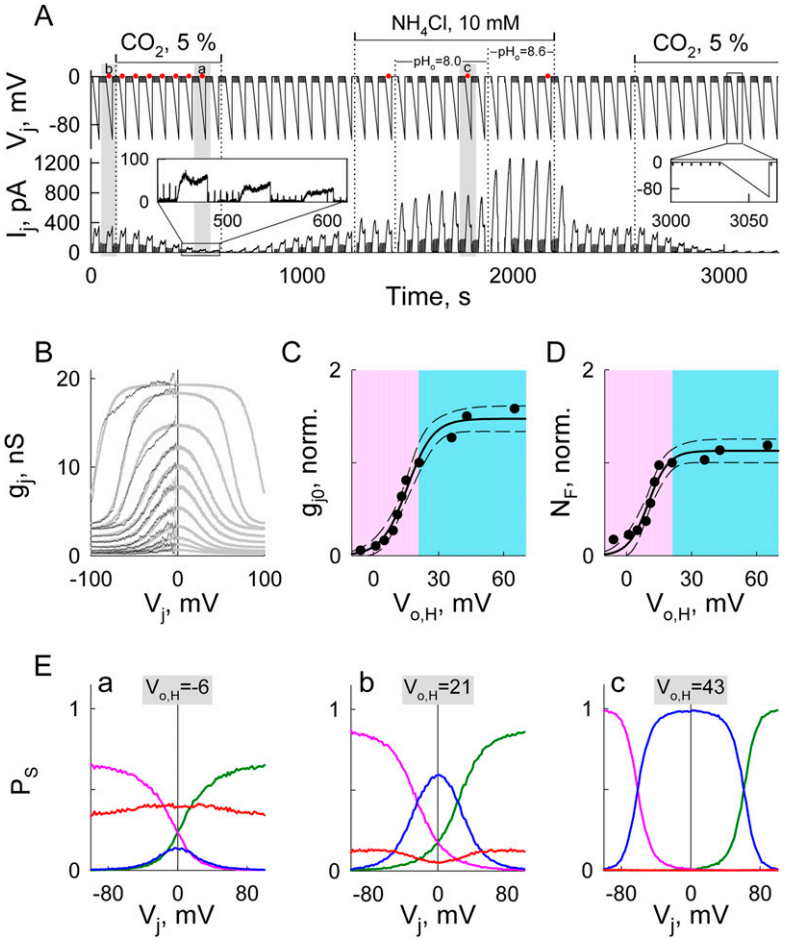

Fig. S3. pH_i-dependent modulation of V_j gating in Cx45 homotypic GJs. (*A*) I_j record in a HeLaCx45 cell pair in response to repeated V_j ramps (31 s duration) from 0 to −100 mV during an exposure to MKR solution saturated with 5% CO_2 or containing NH_4Cl. Initial pH of the MKR solution was 7.4 except where otherwise indicated. Voltage steps of −10 mV were used to follow g_j between V_j ramps (*Right Inset*). Responses at low pH_i are shown at higher gain (*Left Inset*). Responses to the second acidification on the right were very similar. (*B*) Junctional conductance–transjunctional voltage (g_j–V_j) plots (in black) calculated for the V_j ramps marked with red dots in *A*. Fits to the experimental data (gray lines) were calculated assuming symmetry of the g_j–V_j relation. (*C*) Relation between g_js normalized to g_j at V_j = 0 mV under control conditions (g_{j0}, norm.) and the voltage across an apposed hemichannel at which its open probability, $P_{o,H}$, is 0.5 ($V_{o,H}$). Acidic conditions are shown in light pink, and alkaline conditions are shown –in light blue relative to pH_i = 7.2. (*D*) Relation between N_F normalized to N_F at pH_i = 7.2 and $V_{o,H}$. Relations shown in *C* and *D* were obtained from fits in *B*. Solid lines in *C* and *D* are fits to the data using a sigmoidal equation ($y = a/(1+e^{-((x-xo)/b)})$). Dashed lines show 95% confidence intervals (CI). (*E*) Probability that channels dwell in $P_{O\text{-}O}$ (blue), $P_{C\text{-}O}$ (green), $P_{O\text{-}C}$ (pink), and $P_{C\text{-}C}$ (red) states obtained from fitting of records during the ramps *a*–*c* marked with gray rectangles in *A*. Calculated values of $V_{o,H}$ are indicated.

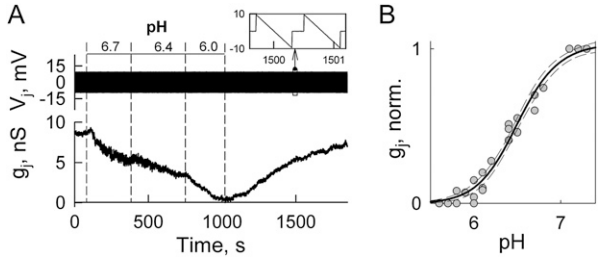

Fig. S4. Effect of pH_i on g_j of Cx43-EGFP homotypic GJs. (*A*) pH_i and g_j measurements in a HeLaCx43-EGFP cell pair during application of 0.5, 2, and 5% CO_2 resulting in pH_i of 6.7, 6.4, and 6.0, respectively. Junctional conductance (g_j) was measured by applying repeated V_j ramps (600 ms in duration) from +10 mV to −10 mV (*Inset*). (*B*) Gray circles show normalized g_j–pH_i dependence of homotypic Cx43-EGFP GJs (n = 7). The solid black curve shows fit to the data (gray circles) of a Hill equation; acid dissociation constant (pK_a) equal 6.50 ± 0.03; Hill coefficient **n** = 1.98. Dashed lines show 95% confidence bands.

Table S1. Parameters of voltage gating obtained from data shown in Figs. 2*B* and 3*B*

Ramp no.	A_H	$V_{o,H}$	$\gamma_{o,H}$	N_F
Figure 2*B*				
1	0.09	23	64	701
2	0.10	21	64	624
3	0.11	19	64	548
4	0.11	17	64	437
5	0.11	12	64	363
6	0.11	11	64	294
7	0.11	7	64	241
8	0.11	3	64	202
9	0.11	0	64	169
10	0.11	−4	64	134
Figure 3*B*				
1	0.11	25	64	948
2	0.11	34	64	1,127
3	0.11	50	64	1,324

aHC, apposed hemichannel; A_H, coefficient characterizing the steepness of $P_{o,H}$ changes as a function of V_H; $\gamma_{o,H}$, single aHC conductance; N_F, number of functional channels; $P_{o,H}$, open probability of aHC; $V_{o,H}$, voltage across aHC at which its $P_{o,H} = 0.5$.

Table S2. Parameters of voltage gating obtained from data shown in Figs. 4*F* and 5*B*

aHC	Ramp #	A_H	$V_{o,H}$	$\gamma_{o,H}$	N_F
Cx45	1	0.11	4	64	113
	2	0.11	10	64	221
	7	0.10	21	64	697
	3	0.11	31	64	849
	4	0.11	39	64	945
	6	0.09	58	64	1056
Cx43-EGFP	1	0.09	30	220	113
	2	0.10	40	220	221
	7	0.10	40	220	697
	3	0.10	50	220	849
	4	0.10	50	220	945
	6	0.09	50	220	1056
Cx45	1	0.10	15	64	1076
	2	0.10	9	64	896
	3	0.10	5	64	781
	4	0.10	3	64	605
	5	0.10	−2	64	483
	6	0.10	−5	64	350
	7	0.10	−8	64	213
	8	0.10	−11	64	108
Cx43- EGFP	1	0.09	75	220	1076
	2	0.09	75	220	896
	3	0.09	75	220	781
	4	0.10	70	220	605
	5	0.10	55	220	483
	6	0.10	46	220	350
	7	0.10	38	220	213
	8	0.10	35	220	108

aHC, apposed hemichannel; A_H, coefficient characterizing the steepness of $P_{o,H}$ changes as a function of V_H; $\gamma_{o,H}$, single aHC conductance; N_F, number of functional channels; $P_{o,H}$, open probability of aHC; $V_{o,H}$, voltage across aHC at which its $P_{o,H} = 0.5$.